sciendo

POLISH MARITIME RESEARCH 1 (105) 2020 Vol. 27; pp. 29-38
10.2478/pomr-2020-0003

PREDICTION OF SHIP MOTIONS VIA A THREE-DIMENSIONAL TIME-DOMAIN METHOD FOLLOWING A QUAD-TREE ADAPTIVE MESH TECHNIQUE

Teng Zhang
Dalian Maritime University, China
Junsheng Ren
Dalian Maritime University, China
Lu Liu
Dongbei University of Finance and Economics, China

ABSTRACT

A three-dimensional (3D) time-domain method is developed to predict ship motions in waves. To evaluate the Froude-Krylov (F-K) forces and hydrostatic forces under the instantaneous incident wave profile, an adaptive mesh technique based on a quad-tree subdivision is adopted to generate instantaneous wet meshes for ship. For quadrilateral panels under both mean free surface and instantaneous incident wave profiles, Froude-Krylov forces and hydrostatic forces are computed by analytical exact pressure integration expressions, allowing for considerably coarse meshes without loss of accuracy. And for quadrilateral panels interacting with the wave profile, F-K and hydrostatic forces are evaluated following a quad-tree subdivision. The transient free surface Green function (TFSGF) is essential to evaluate radiation and diffraction forces based on linear theory. To reduce the numerical error due to unclear partition, a precise integration method is applied to solve the TFSGF in the partition computation time domain. Computations are carried out for a Wigley hull form and S175 container ship, and the results show good agreement with both experimental results and published results.

Keywords: Froude-Krylov forces; adaptive mesh technique; analytical; transient free surface Green function; precise integration method

INTRODUCTION

The design and operation of a ship requires accurate prediction of its wave-induced motions in various sea states. The three-dimensional time-domain methods have remarkable advantages over three-dimensional frequency-domain methods in dealing with forward speed problems, strong nonlinear problems, transient problems, unsteady manoeuvre problems, and so on. Thus, the three-dimensional time-domain methods are widely adopted in engineering application.

For linear methods, incident wave elevation and ship motions are assumed to be small compared with the wave length. The evaluation of F-K forces, hydrostatic forces, radiation forces and diffraction forces is carried out over the mean wetted body surface. Based on the TFSGF method, Beck [1] solved the linearised radiation problem for a hemisphere at zero speed in still water using the linear impulse response functions. King [9] and Datta [4] further studied the linearised diffraction problem for ship motions with steady forward speed by the transient free surface Green function method. The accurate and efficient evaluation of TFSGF is essential to linear formulation for the diffraction and radiation forces. Beck [1] and King [9] applied series expansion and asymptotic expansions to different computational sub-domains due to the properties of the TFSGF. However, the partition between the small computational time sub-domain and the large computational time sub-domain is not clear, which may

lead to considerable loss of accuracy. Clement [3] discovered that the TFSGF is the solution of a fourth-order ordinary differential equation (ODE). Shen [15] solved the ODEs by the fourth-order Runge–Kutta method (RK44), but it leads to numerical instability after a long duration simulation, even for a quite small fixed time step. The precise integration method (PIM) [11], which is much more accurate and stable than the RK44 method for the same time step size, is applied to solve the ODE [10]. However, this method is quite time-consuming due to excessive subdivisions of each time step size and a pretty high order of coefficient matrix.

The key to accurate evaluation of F-K forces and hydrostatic forces is the exact generation of the instantaneous wet hull surface under the incident wave profile, for which dynamic adaptive meshes are considered. Singh [16] adopted the wet-dry method, in which the hull is defined by two sets of panels: the first set of panels is named coarse panels for the mean wet hull surface used to solve the linear hydrodynamic problem; the second set of panels is named fine panels for the full hull used for evaluating F-K forces and hydrostatic forces. At every time instant, if the centroid of the fine panel is under the incident wave profile then it is taken to be wet; otherwise it is considered dry. For dry panels, the pressures are considered to be zero. Thus, the pressure integrations for F-K forces and hydrostatic forces are solved by simply adding each panel's contribution. However, even if the relative position change of the panel is much smaller than the panel size, a panel between two successive time steps may jump from a wet state to a dry state or from a dry state to a wet state, which may show discrete 'jumps' between successive time steps for the evaluation of forces. Sengupta [14] adopted the instantaneous mesh interception scheme to generate the instantaneous wet hull surface under the incident wave profile, in which the full hull is discretised only by coarse panels. He checked for the panels interacting with the incident wave profile, and determined the two intersection points for each panel by a standard least squares iteration method. The exact area of the partially wet panel and its centroid can be solved. This scheme makes the instantaneous wetted hull surface under the incident wave profile vary smoothly and continuously. If the wave height to wave length ratio is large, it is difficult to determine the interaction segments, and the iteration method used to acquire the interaction points is quite time-consuming. Rodrigues [13] proposed a third scheme based on the quad-tree subdivision approach. The third scheme is almost the same as the second scheme, except for the partially wet panel process. Following a quad-tree subdivision approach, such panels are subdivided until a prescribed error limit is reached, and adjacent subpanels of the same tree level are agglomerated. However, agglomerating subpanels of the same level would be a troublesome step, and the algorithm is quite complex.

To accurately predict ship motions in regular waves, the adaptive mesh technique in light of a quad-tree subdivision scheme is adopted for generation of the instantaneous wet hull surface. For panels under both an instantaneous incident wave profile and a mean free surface, F-K and hydrostatic forces are calculated by analytical integration expressions on quadrilateral panels without loss of accuracy. For panels interacting with the instantaneous wave profile where F-K forces are significantly obvious and vary a lot, based on the quad-tree subdivision, such panels are subdivided into smaller subpanels until the prescribed precision is achieved. Due to the large memory of the computer and simplified procedures, there is no need to agglomerate adjacent subpanels of the same tree level, and the F-K and hydrostatic forces on subpanels are evaluated by Gaussian quadrature. Thus, the full hull can be discretised with coarse meshes for the evaluation of the nonlinear F-K and hydrostatic forces. Based on the TFSGF method, perturbation forces are still evaluated on the mean wet hull surface. To reduce the numerical error of TFSGF evaluation, the precise integration method is adopted for the partition computational domain between a small value of the time sub-domain and a large value of the time sub-domain. Finally, a Wigley hull and S175 container ship are used to validate the proposed ship motion model.

MATHEMATICAL FORMULATION

The fluid domain Ω is enclosed by free surface *SF*, body surface S_B and infinite surface S_∞, as shown in Fig. 1. The reference coordinate system *oxyz* is chosen, in which the plane *oxy* is coincident with the mean free surface and the positive direction of the *oz* axis is upward; and the reference system oxyz is moving with the ship at a constant speed *U* along the positive *ox* axis in an incident wave field.

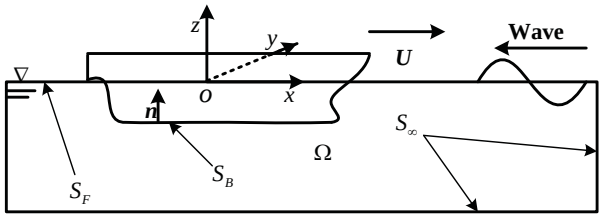

Fig. 1. Ship coordinate systems and fluid domain definition

THE HYDRODYNAMIC PROBLEM

Boundary value equation

Based on potential flow theory, the hydrodynamic problem is formulated in the infinite fluid depth. In reference coordinate system *oxyz*, the total velocity potential in the fluid domain is written as [9]

$$\phi(\boldsymbol{r};t) = -Ux+\phi_S(\boldsymbol{r}) + \phi_I(\boldsymbol{r};t) + \sum_{k=1}^{7}\phi_k(\boldsymbol{r};t) \quad (1)$$

where $-Ux+\phi_S(\boldsymbol{r})$ is the steady wave potential due to steady forward speed; ϕ_I is the incident wave potential; $\phi_k(k = 1,2,\cdots,6)$ is the radiation potential; ϕ_k is the diffraction potential; and $\boldsymbol{r} = (x, y, z)$ is the position vector.

The perturbation potentialsatisfies the following conditions:

$$\begin{cases} \nabla^2\phi_k(\boldsymbol{r};t)=0, & \text{where } \boldsymbol{r}\in\Omega \\ \frac{\partial^2\phi_k}{\partial t^2}+g\frac{\partial\phi_k}{\partial z}=0, & \text{on } z=0 \\ \frac{\partial\phi_k}{\partial \boldsymbol{n}}=m_k\zeta_k+n_k\dot{\zeta}_k, & k=1,2,\cdots,6 \\ \frac{\partial\phi_k}{\partial \boldsymbol{n}}=-\frac{\partial\phi_I}{\partial \boldsymbol{n}}, & k=7 \\ \nabla\phi_k(\boldsymbol{r};t)\to 0, & \text{as } \sqrt{x^2+y^2}\to\infty, z\to-\infty \\ \phi_k=0 \text{ and } \frac{\partial\phi_k}{\partial \boldsymbol{t}}=0, & \text{at } t=0 (k=1,2,\cdots,6) \\ \phi_k=0 \text{ and } \frac{\partial\phi_k}{\partial \boldsymbol{t}}=0, & \text{at } t=-\infty (k=7) \end{cases} \quad (2)$$

where $\boldsymbol{n}$ is the unit normal vector pointing out of the fluid domain; ξ_κ is unsteady motion in the kth mode; $\boldsymbol{n}=(n_1, n_2, n_3)$; $\boldsymbol{r}\times\boldsymbol{n}=(n_4, n_5, n_6)$; $(m_1, m_2, m_3)=(0,0,0)$; $(m_4, m_5, m_6)=(0, U_{n3}-U_{n2})$; [9]; g is the acceleration of gravity.

The TFSGF is used to solve the perturbation potentialand given as [17]

$$G(P,Q;t-\tau)=G^0(P;Q)\delta(t-\tau)+\tilde{G}(P,Q;t-\tau)H(t-\tau) \quad (3)$$

where $\delta(t)$ is the Dirac function; $H(t)$ is the Heaviside unit step function; $P(x, y, z)$ is a field point; $Q(\zeta,n,\xi)$is a source point; τ is the retard time; $G^0=1/r-1/r'$ is the Rankine part of TFSGF; $r=|P-Q|$; $r'=|P'-Q'|$; $Q'(\zeta,n,-\zeta)$ is the image point of Q above the mean free surface; $\tilde{G}$ is the memory part of TFSGF and given by

$$\tilde{G}(P,Q;t-\tau)=2\int_0^\infty\sqrt{gK}\,e^{K(z+\zeta)}\sin\left[\sqrt{gK}(t-\tau)\right]J_0(KR)\,dK \quad (4)$$

where J_0 is a Bessel function of order zero.

G^0 and its derivative integrations over the quadrilateral panels can be solved by the Hess-Smith method [5]. $\tilde{G}$ and its derivatives can be solved in section 3.1.

The boundary value equation of perturbation potential Φ_κ can be given by [9]

$$\begin{aligned} &2\pi\phi_k(P;t)+\iint_{S_B}\phi_k(Q;t)\frac{\partial G^0}{\partial \boldsymbol{n}_Q}dS=\iint_{S_B}G^0\frac{\partial\phi_k(Q;t)}{\partial \boldsymbol{n}_Q}dS+ \\ &\int_{t_0}^t d\tau\iint_{S_B}\tilde{G}(P,Q;t-\tau)\frac{\partial\phi_k(Q;\tau)}{\partial \boldsymbol{n}_Q}-\phi_k(Q;\tau)\frac{\partial\tilde{G}(P,Q;t-\tau)}{\partial \boldsymbol{n}_Q}dS \\ &+\frac{U^2}{g}\int_{t_0}^t d\tau\oint_{\Gamma_0}\tilde{G}(P,Q;t-\tau)\frac{\partial\phi_k(Q;\tau)}{\partial\xi}-\phi_k(Q;\tau)\frac{\partial\tilde{G}(P,Q;t-\tau)}{\partial\xi}d\eta \\ &+\frac{U}{g}\int_{t_0}^t d\tau\oint_{\Gamma_0}\phi_k(Q;\tau)\frac{\partial\tilde{G}(P,Q;t-\tau)}{\partial\tau}d\eta \end{aligned} \quad (5)$$

where Γ_0 is the intersecting line between the mean wet body surface S_B and the mean free surface S_F; t_0 is the initial time; $\boldsymbol{n}_Q$ is a unit normal vector pointing out of the fluid domain at source point Q.

Eq. (5) for the perturbation potential Φ_κ can be solved by the constant panel method, and the trapezoidal rule is used for convolution integration.

The hydrodynamic problem formulation

Based on the impulse response method, the radiation potential Φ_k can be written as [1]

$$\phi_k(P;t)=\int_{t_0}^t\hat{\phi}_k(P;t-\tau)\dot{\zeta}_k(\tau)d\tau \quad (6)$$

where $\hat{\phi}_k(P;t)$ is the impulse response radiation potential in the kth mode. $\hat{\phi}_k(P;t)$ is decomposed into

$$\hat{\phi}_k(P;t)=\psi_{1k}(P)\delta(t)+\psi_{2k}(P)H(t)+\chi_k(P;t) \quad (7)$$

Thus, the expression can be obtained for radiation forces F_{jk} as

$$F_{jk}(t)=-a_{jk}\ddot{\zeta}_k(t)-b_{jk}\dot{\zeta}_k(t)-c_{jk}(t)\zeta_k(t)-\int_0^t K_{jk}(t-\tau)\dot{\zeta}_k(\tau)d\tau \quad (8)$$

where F_{jk} is the radiation force in the jth mode due to the kth mode motion; ρ is the density of fluid $K_{jk}(t)=\rho\iint_{S_B}(\frac{\partial\chi_k}{\partial t}n_j-\chi_k m_j dS)$; $a_{jk}=-\rho\iint_{S_B}\psi_{1k}n_j dS$; $c_{jk}=-\rho\iint_{S_B}\psi_{2k}m_j dS$; $b_{jk}=\rho\iint_{S_B}(\psi_{1k}m_j-\psi_{2k}n_j)dS$.

The added mass $A_{jk}(\omega)$ and damping coefficients $B_{jk}(\omega)$can be obtained via Fourier transform with coefficients a_{jk}, b_{jk}, c_{jk} and K_{jk} in the time-domain (j = 1,2, ⋯ ,6; j = 1,2, ⋯ ,6; ω is the circular frequency) [9].In the reference coordinate system oxyz, the incident wave potentialis given by

$$\phi_I(P;t)=\frac{i\eta_0 g}{\omega}e^{K[z-i(x\cos\alpha+y\sin\alpha)]}e^{i\omega_e t} \quad (9)$$

where η_0 is the wave amplitude; α is the wave propagation angle ($\alpha=\pi$ is head seas); $K=\omega^2/g$ is the wave number; $\omega_e=\omega-KU\cos\alpha$ is the encounter frequency.

The incident wave elevation $\eta_I(t)$ at the origin o is given by

$$\eta_I(t)=\eta_0 e^{i\omega_e t} \quad (10)$$

Based on the impulse response function method [1], $\hat{K}(P;t)$ is the impulse response function of incident wave velocity $\nabla\phi_I(P;t)$, $\hat{\phi}_7(P;t)$ is the impulse response function of $\phi_7(P;t)$, and $K_{j7}(t)$ is the impulse response function of diffraction force $F_{j7}(t)$ (j = 1,2, ⋯ ,6); $\hat{K}(P;t)$, $\hat{\phi}_7(P;t)$ and $K_{j7}(t)$ are given respectively by

$$\nabla\phi_I(P;t)=\int_{-\infty}^{+\infty}\hat{K}(P;t-\tau)\eta_I(\tau)d\tau \quad (11)$$

$$\phi_7(P;t)=\int_{-\infty}^{+\infty}\hat{\phi}_7(P;t-\tau)\eta_I(\tau)d\tau \quad (12)$$

$$F_{j7}(t)=\int_{-\infty}^{+\infty}K_{j7}(t-\tau)\eta_I(\tau)d\tau \quad (13)$$

In combination with Eqs. (2), (5), (11) and (12), the K_{j7} can be obtained. Thus, the diffraction force $F_{j7}(t)$ can be solved.

EVALUATION FOR F-K FORCES

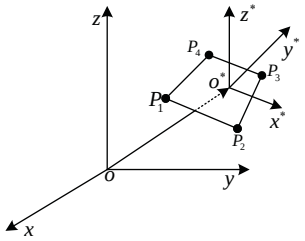

Fig. 2. Reference coordinate system and panel coordinate system

Consider the two coordinate systems illustrated in Fig. 2: the reference coordinate system $o^*x^*y^*z^*$ and the local panel coordinate systemdefined by the vertices 1 to 4 in the counterclockwise direction, named P_1, P_2, P_3 and P_4 respectively. The o^*z^* axis points positively to the exterior of the fluid. The transformation between the position vector $\boldsymbol{r}$ in the reference coordinate system *oxyz* and the position vector in the panel coordinate system $o^*x^*y^*z^*$ is given by

$$\boldsymbol{r} = \boldsymbol{r_0} + \boldsymbol{T}\boldsymbol{r}^* \tag{14}$$

where $\boldsymbol{r}_0 = (x_0, y_0, z_0)$ is the position vector in the reference coordinate system oxyz, which is the origin of the panel coordinate system $o^*x^*y^*z^*$; $\boldsymbol{T}$ is the unit transformation cosine-director matrix between $o^*x^*y^*z^*$ and the *oxyz* system and is given as

$$\boldsymbol{T} = \begin{bmatrix} \langle \boldsymbol{x}^*, \boldsymbol{x} \rangle & \langle \boldsymbol{y}^*, \boldsymbol{x} \rangle & \langle \boldsymbol{z}^*, \boldsymbol{x} \rangle \\ \langle \boldsymbol{x}^*, \boldsymbol{y} \rangle & \langle \boldsymbol{y}^*, \boldsymbol{y} \rangle & \langle \boldsymbol{z}^*, \boldsymbol{y} \rangle \\ \langle \boldsymbol{x}^*, \boldsymbol{z} \rangle & \langle \boldsymbol{y}^*, \boldsymbol{z} \rangle & \langle \boldsymbol{z}^*, \boldsymbol{z} \rangle \end{bmatrix} \tag{15}$$

where $\boldsymbol{x}$, $\boldsymbol{y}$ and $\boldsymbol{z}$ are unit base vectors for the *oxyz* system; $\boldsymbol{x}^*$, $\boldsymbol{y}^*$ and $\boldsymbol{z}^*$ are unit base vectors for the $o^*x^*y^*z^*$ system; $\langle , \rangle$ stands for the internal product between base vectors..

Based on linear dynamic conditions, the incident wave elevation $\eta_I(t)(z \le 0)$ is

$$\eta_I(t) = \eta_0 \cos[\omega_e t - K(x\cos\alpha + y\sin\alpha)] \tag{16}$$

From the linearised Bernoulli equation, the incident wave pressure p_I and hydrostatic pressure p_H can be $p_I(t) = \rho g \eta_I(t) e^{Kz}$ and $p_H = \rho g z$ respectively ($z \le 0$) [2].

The pressure p_{IH} composed of $p_I(t)$ and p_H can be given by

$$p_{IH}(t) = \rho g \eta_I(t) e^{Kz} - \rho g z (z \le 0) \tag{17}$$

The F-K forces and hydrostatic forces should be obtained over the instantaneous wet hull surface, and p_{IH} should be modified to satisfy the free surface condition [2].

The F-K forces and hydrostatic forces acting on the body in the ith mode in the reference system *oxyz* are given by

$$F_{iIH}(t) = \iint_{S_I(t)} p_{IH}(t) n_i \mathrm{d}S \tag{18}$$

where F_{iIH} is the combination of the incident wave force and hydrostatic force in the *i*th mode solved on the instantaneous wetted hull surface $S_I(t)$ which is under the instantaneous wave profile.

F-K forces based on analytical integration expression

The full hull is discretised by *N* coarse quadrilateral panels. For the ith quadrilateral panel under both the instantaneous wave profile and mean free surface, the F-K force F_{Ii} is given by

$$\boldsymbol{F}_{Ii} = \boldsymbol{n}_i \rho g \eta_0 \iint_{S_i} e^{Kz} \cos[\omega_e t - K(x\cos\alpha + y\sin\alpha)] \mathrm{d}S \tag{19}$$

where S_i is the area of the ith quadrilateral panel, and $\boldsymbol{n}_i$ is the unit normal vector of the *i*th quadrilateral panel pointing out of the fluid.

Note that Eq. (19) can be rewritten in terms of the *i*th panel coordinate system $o^*x^*y^*z^*$

$$\boldsymbol{F}_{Ii} = \boldsymbol{n}_i \rho g \eta_0 \iint_{S_i} e^{\mathrm{B}(x^*, y^*)} \mathrm{cosA}(x^*, y^*) \mathrm{d}S \tag{20}$$

where

$$\begin{aligned} \mathrm{A}(x^*, y^*) = {} & \omega_e t - K[(x_0 + \langle \boldsymbol{x}^*, \boldsymbol{x} \rangle x^* + \\ & \langle \boldsymbol{y}^*, \boldsymbol{x} \rangle y^*)\cos\alpha + (y_0 + \langle \boldsymbol{x}^*, \boldsymbol{y} \rangle x^* + \langle \boldsymbol{y}^*, \boldsymbol{y} \rangle y^*)\sin\alpha] \end{aligned} \tag{21}$$

$$\mathrm{B}(x^*, y^*) = K(z_0 + \langle \boldsymbol{x}^*, \boldsymbol{z} \rangle x^* + \langle \boldsymbol{y}^*, \boldsymbol{z} \rangle y^*) \tag{22}$$

The *j*th edge of the ith quadrilateral panel can be parameterised by (*j*=1,2,3,4)

$$g_{ij}(\upsilon) = \left(x^*_{0,ij}, y^*_{0,ij}\right) + \left(\Delta x^*_{0,ij}, \Delta y^*_{0,ij}\right)\upsilon, \upsilon \in [0,1] \tag{23}$$

where $\Delta x^*_{ij} = x^*_{1,ij} - x^*_{0,ij}, \Delta y^*_{ij} = y^*_{1,ij} - y^*_{0,ij}$, $x^*_{0,ij} = x^*_{ij}(0); x^*_{1,ij} = x^*_{ij}(1), y^*_{0,ij} = y^*_{ij}(0)$ and $y^*_{1,ij} = y^*_{ij}(1)$.

A, B on the *j*th side of the *i*th panel can be expressed as with respect to parameter υ

$$\begin{aligned} \mathrm{B}_{ij}(\upsilon) = {} & K\left[z_0 + \langle \boldsymbol{x}^*, \boldsymbol{z} \rangle \left(x^*_{0,ij} + \Delta x^*_{ij}\upsilon\right) + \right. \\ & \left. \Delta x^*_{ij}\upsilon\right) + \langle \boldsymbol{y}^*, \boldsymbol{z} \rangle \left(y^*_{0,ij} + \Delta y^*_{ij}\upsilon\right)\Big] \end{aligned} \tag{24}$$

$$\mathrm{A}_{ij}(\upsilon)=\omega_e t-K\left\{\begin{bmatrix}x_0+\langle \boldsymbol{x}^*,\boldsymbol{x}\rangle\left(x^*_{0,ij}+\Delta x^*_{ij}\upsilon\right)\\ +\langle \boldsymbol{y}^*,\boldsymbol{x}\rangle\left(y^*_{0,ij}+\Delta y^*_{ij}\upsilon\right)\end{bmatrix}\cos\alpha+\begin{bmatrix}y_0+\langle \boldsymbol{x}^*,\boldsymbol{y}\rangle\left(x^*_{0,ij}+\Delta x^*_{ij}\upsilon\right)\\ +\langle \boldsymbol{y}^*,\boldsymbol{y}\rangle\left(y^*_{0,ij}+\Delta y^*_{ij}\upsilon\right)\end{bmatrix}\sin\alpha\right\} \tag{25}$$

$A_{v,ij}(\upsilon)$ is the derivative of $A_{ij}(\upsilon)$ with respect to υ, and $B_{v,ij}(\upsilon)$ is the derivative of $B_{ij}(\upsilon)$ with respect to υ

Let $\Psi_\upsilon=\mathrm{A}_\upsilon^2+\mathrm{B}_\upsilon^2$, and

$$CE=\begin{cases}\frac{e^{\mathrm{B}}(\mathrm{B}_\upsilon\cos\mathrm{A}+\mathrm{A}_\upsilon\sin\mathrm{A})}{\Psi_\upsilon}, & \Psi_\upsilon\neq 0\\ e^{\mathrm{B}}\upsilon\cos\mathrm{A}, & \Psi_\upsilon=0\end{cases},SE=\begin{cases}\frac{e^{\mathrm{B}}(\mathrm{B}_\upsilon\sin\mathrm{A}-\mathrm{A}_\upsilon\cos\mathrm{A})}{\Psi_\upsilon}, & \Psi_\upsilon\neq 0\\ e^{\mathrm{B}}\upsilon\sin\mathrm{A}, & \Psi_\upsilon=0\end{cases} \tag{26}$$

$A_{x^*,i}$ and $A_{y^*,i}$ are A's derivatives on the i th panel and can be expressed with respect to parameter x^* and y^* respectively, and $B_{x^*,i}$ and $B_{y^*,i}$ are B's derivatives on the ith panel and can be expressed with respect to parameter x^* and y^* respectively. Let $\Psi_{x^*}=\mathrm{A}^2_{x^*}+\mathrm{B}^2_{x^*}$, $\Psi_{y^*}=\mathrm{A}^2_{y^*}+\mathrm{B}^2_{y^*}$. Applying Green's Theorem with parameterisation in Eq. (23), and resorting to integration by parts, if $\Psi_{x^*}\neq 0$, Eq. (20) can be expressed as

$$\boldsymbol{F}_{Ii}=\frac{\boldsymbol{n}_i\rho g\eta_0}{\Psi_{x^*}}\sum_{j=1}^{4}\Delta y^*_{ij}\int_0^1 e^{\mathrm{B}_{ij}(\upsilon)}\left[\mathrm{B}_{x^*,i}\cos\mathrm{A}_{ij}(\upsilon)+\mathrm{A}_{x^*,i}\sin\mathrm{A}_{ij}(\upsilon)\right]d\upsilon \tag{27}$$

ΔCE_{ij} is to be understood as as$[CE_{ij}(1)-CE_{ij}(0)]$ and ΔSE_{ij} is to be understood as $[SE_{ij}(1)-SE_{ij}(0)]$ $\boldsymbol{F}_{Ii}$ can be given as

$$\boldsymbol{F}_{Ii}=\frac{\boldsymbol{n}_i\rho g\eta_0}{\Psi_{x^*}}\sum_{j=1}^{4}\Delta y^*_{ij}\left[\mathrm{B}_{x^*,i}\Delta CE_{ij}+\mathrm{A}_{x^*,i}\Delta SE_{ij}\right] \tag{28}$$

If $\Psi_{y^*}\neq 0$ $\boldsymbol{F}_{Ii}$ can be solved the same as $\Psi_{x^*}\neq 0$ directly

Note that the analytical integration expressions for hydrostatic forces, hydrostatic moments and F-K moments can be solved in a similar manner.

F-K forces evaluation based on quad-tree subdivision scheme

There are three types of panels states for the full hull: 1) fully dry panel, in which all of the panel is above the incident wave profile; 2) fully wet panel, in which all of the panel is below the incident wave profile; 3) partially wet panel, in which part of the panel is under the incident wave profile. Partially wet panels, due to the large amplitude of the incident wave and large F-K forces variation, should be subdivided following a quad-tree subdivision as shown in Fig. 3.

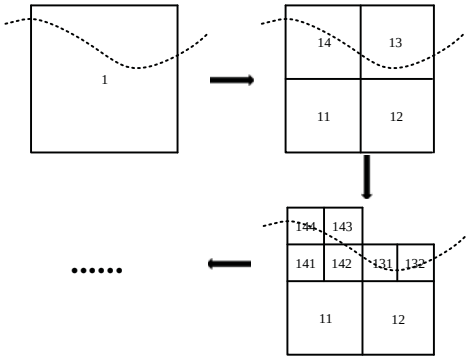

Fig. 3. Quad-tree subdivision for a partially wet panel

1) Check for the partially wet panel at each time step, if true, proceed to step 2. Otherwise the panel is eliminated if it is a fully dry panel, if not, the F-K pressures integration on the fully wet panel can be solved numerically and accurately by a 2 × 2 points Gaussian quadrature formula.

2) Subdivide the partially wet panel into four smaller subpanels, and check for fully dry panels, fully wet panels and partially wet panels from the newly obtained subpanels respectively. From the partially wet subpanels, if the centre of each partially wet subpanel is below the incident wave profile, it is considered to be a fully wet panel, and otherwise is taken as a fully dry panel.

3) Add the contribution over each fully wet subpanel of the same level to solve the F-K pressures integration. For example, as shown in Fig. 3, the panels labelled '11' and '12' are the same tree level. Add the F-K pressure integration contribution from the different tree level.

4) Compare the F-K pressures integration between two successive subdivisions. If the relative error is less than the prescribed error limit, stop subdividing the partially wet panels, if not, proceed to step 2.

SOLVING THE EQUATIONS OF MOTIONS

Using Newton's Second Law, the six degrees of freedom motions of the rigid body in fixed space are determined by

$$M_{ij}\ddot{\zeta}_j(t)=F_i(t) \tag{29}$$

where $F_i(t)=F_{iIH}(t)+F_{i7}(t)+\sum_{j=1}^{6}F_{ij}(t)$, and Eq. (29)can be given as

$$\left(M_{ij}+a_{ij}\right)\ddot{\zeta}_j(t)+b_{ij}\dot{\zeta}_j(t)+c_{jk}(t)\zeta_j(t)+\int_0^t K_{ij}(t-\tau)\dot{\zeta}_j(\tau)d\tau=F_{iIH}(t)+F_{i7}(t) \tag{30}$$

Eq. (30) can be solved by the Runge–Kutta method. Finally, the time history of ship motions can be obtained.

COMPUTATIONS AND RESULTS VALIDATION

3.1 THE EVALUATION AND ANALYSIS OF TFSGF

Eq. (4) can be transformed into non-dimensional form

$$\tilde{G}(P,Q;t-\tau)=2\sqrt{g/\left(r^{'}\right)^{3}}\,F(\mu,\beta) \tag{31}$$

Let $\lambda = Kr^{'}$, $\mu = -(z+\zeta)/r^{'}$ and $\beta = (t-\tau)\sqrt{g/r^{'}}$. $F(\mu,\beta)$ is given by

$$F(\mu,\beta)=\int_0^{\infty}\sqrt{\lambda}\mathrm{e}^{-\lambda\mu}\sin\left[\beta\sqrt{\lambda}\right]J_0\left(\lambda\sqrt{1-\mu^2}\right)\mathrm{d}\lambda \tag{32}$$

$F(\mu,\beta)$ is a solution to the following fourth-order ordinary differential equation

$$\frac{\partial^4 F}{\partial\beta^4}+\mu\beta\frac{\partial^3 F}{\partial\beta^3}+\frac{(\beta^2+16\mu)}{4}\frac{\partial^2 F}{\partial\beta^2}+\frac{7\beta}{4}\frac{\partial F}{\partial\beta}+\frac{9F}{4}=0 \tag{33}$$

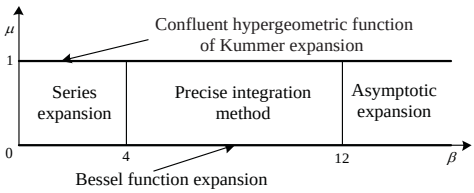

Fig. 4. Computation domains for evaluation of TFSGF

For small values of β, the series expansion can be adopted to solve the TFSGF, while for large values of β, the asymptotic expansion can be used to solve the TFSGF [1,9]. However, the partition domain is not clear between the small values of the β computation domain and large values of the β computation domain, for which the numerical accuracy of the TFSGF reduces a lot. Huang took $\beta = 8 + 1.515\mu$ as the dividing line [6], where the partition domain is in the range 8~9.515. And a number of other researchers usually take 6~8 as the partition domain for β. In the present study, to solve Eq. (33), 4~12 is taken to be the partition computational domain in which the precise integration method (PIM) is adopted [11], while the fourth-order Runge–Kutta method (RK44) is adopted by Shen [15]. For different computational domains, different computation methods are adopted, as illustrated in Fig. 4.

The fourth-order ordinary differential equation Eq. (33) can be written as a system of first-order equations

$$\dot{\widetilde{\boldsymbol{X}}}(\beta)=\widetilde{\boldsymbol{A}}(\beta)\widetilde{\boldsymbol{X}}(\beta) \tag{34}$$

where $\widetilde{\boldsymbol{X}}(\beta)=[F \quad \partial F/\partial\beta \quad \partial^2 F/\partial\beta^2 \quad \partial^3 F/\partial\beta^3]$and

$$\widetilde{\boldsymbol{A}}(\beta)=\begin{bmatrix}0 & 1 & 0 & 0\\ 0 & 0 & 1 & 0\\ 0 & 0 & 0 & 1\\ -\frac{9}{4} & -\frac{7\beta}{4} & -4\mu-\frac{\beta^2}{4} & -\mu\beta\end{bmatrix} \tag{35}$$

The initial conditions for Eq. (34) can be solved by series expansion with proper truncation error.

For $\beta\in[\beta_k,\beta_{k+1}]$, let $s=\frac{\beta-\beta_k}{\beta_{k+1}-\beta_k}$ ($s\in[0,1]$), then the relationship between the time variant system and unit time variant system in Eq. (34) is given by

$$\begin{cases}\widetilde{\boldsymbol{X}}[\beta_k+s(\beta_{k+1}-\beta_k)]=\widetilde{\boldsymbol{x}}(s)\\ \widetilde{\boldsymbol{A}}[\beta_k+s(\beta_{k+1}-\beta_k)]=\boldsymbol{A}(s)\end{cases} \tag{36}$$

where $\boldsymbol{A}(s)=\sum_{i=0}^{2}\boldsymbol{A}_i s^i$ ($\boldsymbol{A}_i$ is the time invariant coefficients matrix). The transformation relationship is

$$\mathrm{d}\widetilde{\boldsymbol{x}}/\mathrm{d}s=(\beta_{k+1}-\beta_k)\boldsymbol{A}(s)\widetilde{\boldsymbol{x}}(s) \tag{37}$$

Plugging Eq. (37) into (34), Eq. (34) can be solved by PIM [10].

When $\mu = 0$, the analytical expression of the TFSGF is

$$F(0,\beta)=\frac{\pi\beta^3}{16\sqrt{2}}\left[J_{\frac{1}{4}}\left(\frac{\beta^2}{8}\right)\cdot J_{-\frac{1}{4}}\left(\frac{\beta^2}{8}\right)+J_{\frac{3}{4}}\left(\frac{\beta^2}{8}\right)\cdot J_{-\frac{3}{4}}\left(\frac{\beta^2}{8}\right)\right] \tag{38}$$

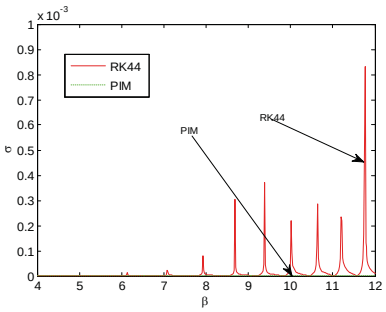

Fig. 5. Diagram of relative errorofcompared with analytical results

To compare the numerical accuracy of PIM with RK44 in the partition computational domain, the value of $\widetilde{\boldsymbol{X}}$ (4) is solved by PIM and is set to the initial conditions for Eq. (34). When $\mu = 0$, the time-step is set as 0.02, and the TFSGF can be solved by PIM, RK44 and the analytical method respectively. The numerical results obtained from both PIM and RK44 are compared to the analytical results, and the absolute relative error is denoted as σ.

From Fig. 5, in the partition computational domain 4~12, the numerical error of PIM is much lower than RK44. Thus, the PIM has great numerical advantages over RK44 in solving the TFSGF in the partition computational domain.

THE HYDRODYNAMIC RESULTS AND ANALYSIS

The principal dimensions of a Wigley I hull and S175 container ship are given in Table 1 [7,16].

Tab.1. Principal dimensions of Wigley I hull and S175 container ship

Hull	L(m)	B(m)	D(m)	∇(m^3)	kyy/L
Wigley I hull	3.0	0.3	0.1875	0.0946	0.25
S175 container ship	175	24	9.5	24140	0.24

The upper hull above the mean waterline of the Wigley I hull is vertical, and the meshes of the full hull are illustrated in Fig. 6.

Fig. 6. Panels distribution on Wigley I hull

The Wigley I hull is studied at Froude number Fn=0.2 in head seas ($\alpha = \pi$). Figs. 7~8 show non-dimensional hydrodynamic coefficients for the Wigley I hull. The experimental results are denoted as "Experiment", the computational results obtained by the present method are denoted as "Present method", and the computational results obtained by Magee are denoted as "Magee" [12].

The non-dimensional hydrodynamic coefficients are defined as $A_{33}^{'} = A_{33}/(\rho\nabla)$, $A_{55}^{'} = A_{55}/(\rho\nabla L^2)$, $B_{33}^{'} = \sqrt{L/g}\,B_{33}/(\rho\nabla)$ and $B_{55}^{'} = \sqrt{L/g}\,B_{55}/(\rho\nabla L^2)$ respectively. The non-dimensional frequency is defined as $\omega^{'} = \omega\sqrt{L/g}$.

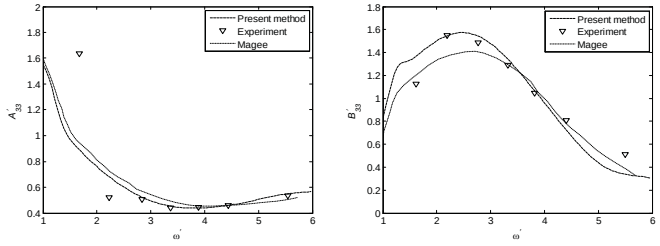

Fig. 7. Non-dimensional heave added mass and damping coefficients

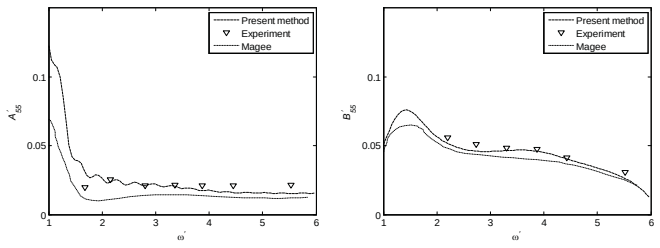

Fig. 8. Non-dimensional pitch added mass and damping coefficients

From Figs. 7~8, the hydrodynamic coefficients by the present method are closer to the experimental results than Magee's. The numerical prediction of the damping coefficients is better than that of the added mass coefficients. In the low frequency range, the computational results have a greater deviation from the experimental results due to the singularity of the critical frequency.

THE GENERATION OF EXACT INSTANTANEOUS HULL SURFACE

The Wigley I hull advances at Froude number Fn=0.2 in head seas, the amplitude of the incident wave η_0 is 0.036 m, and the wave length to length between particular ratio λ/l is 1.4..

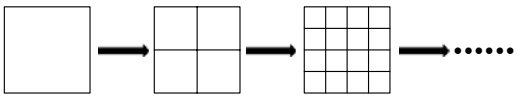

Fig. 9 Panel subdivision diagram

Selecting a square panel under the mean free surface, the coordinates of the four vertices in the reference coordinate system $oxyz$ are P_1 (-0.5, 0, -1), P_2 (0.5, 0, -1), P_3 (0.5, 0, 0) and P_4 (-0.5, 0, 0). At time instant t=0, the F-K pressure integration over the square panel by the analytical expression method mentioned in section 2.2.1 is 170.738 N (the precision is set to 0.001N). Also, the F-K pressure integration over the square panel can also be obtained by the Gauss numerical integral. The prescribed precision for the Gauss numerical integral can be obtained by progressively subdividing the square panel as shown in Fig. 9. The F-K pressure integration on each subpanel can be evaluated by 2 × 2 points Gaussian quadrature.

Tab. 2. Values of F-K pressure integration on the panels at t=0 (unit: N)

Subdivision time	**0**	**1**	**2**	**3**
F-K pressure integration	170.341	170.714	170.737	170.738

From Table 2, when the subdivision time is 3, the square panel is subdivided into 64 smaller subpanels, and the computational result of the Gauss numerical integral for F-K forces is the same as the analytical integration. However, the number of panels required for the analytical integration method is much less than for the Gauss numerical integral method, which improves the computational efficiency without loss of accuracy. If the geometry of the ship body under the waterline is simple, the magnitude for the discretisation of the hull can be of $O(10)$, which are extremely coarse meshes without loss of accuracy. For example, only six panels are needed for the initial mesh of a simple barge.

This paper presents a coarse grid of 80 × 8 for the Wigley I's full hull, and panels interacting with the instantaneous incidental wave profile should be subdivided by the quad-tree subdivision scheme as shown in Fig. 3, named scheme 1. Singh presents a fine grid which subdivides each original coarse panel into 4 smaller subpanels; the fine grid is 160 × 16over the full hull, named scheme 2 [16]. Panels interacting with the instantaneous incidental wave profile, as shown in Fig. 11, should be progressively subdivided until the F-K pressure integrations do not change at all. The obtained numerical

results of F-K pressure integrations can be regarded as the reference, named scheme 3.

Tab.3. Values of F-K pressure integration on the panels of Wigley I hull at t=0 (unit: N)

Panel	scheme 1	scheme 2	scheme 3
pan1	-0.3947	-0.3575	-0.3947
pan2	-0.1777	-0.1652	-0.1777
pan3	0.0772	0.0000	0.0772

For a coarse grid, there are an arbitrary three panels interacting with the instantaneous wave profile at t=0, named pan1, pan2 and pan3 respectively. The pan1, pan2 and pan3 centre coordinates are (1.4625, 0.0084, -0.0234), (1.4625, 0.0650, -0.0234), and (0.8625, 0.1069, 0.0234) in *oxyz* at t=0. The absolute error for F-K pressure integration is set as O(10-4).

From Table 3, the computational results of scheme 1 are much closer to scheme 3 than scheme 2. For scheme 2, the grid for F-K forces evaluation is denser than the perturbation forces, but for panels located around the instantaneous wave profile where the F-K forces are significantly obvious, the number of panels is not enough to achieve accurate results. For scheme 1, the scale of panels for F-K forces evaluation is the same as the perturbation forces, but the panels interacting with the instantaneous wave profile continue to be subdivided by the quad-tree subdivision scheme as mentioned in section 2.2.2. The subdivision for all coarse panels is avoided, which could reduce the computational time. On the other hand, the great value and variation of F-K forces over the panels interacting with the instantaneous wave profile is considered. Finally, the exact F-K forces over each panel can be obtained.

The meshes of the full hull for the S175 container ship are illustrated in Fig. 10.

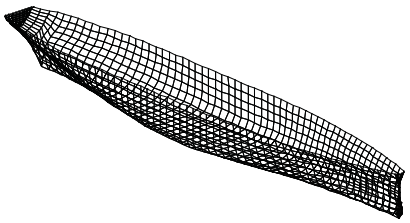

Fig. 10. Panels distribution on S175 container ship hull

The S175 container ship is fixed in the reference system *oxyz* advancing at Froude number Fn =0.0 in head seas, the amplitude of the incident wave η_0 is 5 .0m, and the wave length to length between particular ratio λ/l is 1.

This paper presents scheme 1, scheme 2 and scheme 3 for the mesh generation of the S175 container ship's full hull, which is the same as the Wigley I's full hull. The coarse grid is 100 × 16 over the full hull by scheme 1. The fine grid is 200 × 32 over the full hull by scheme 2. Scheme 3 is still regarded as the reference. The numerical results of scheme 4 are obtained based on the three-dimensional time domain linear method [13].

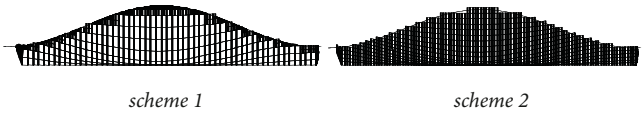

Fig. 11. Panel distribution of S175 container ship under instantaneous incident wave profile at t=0

From Fig. 11, the edge of the instantaneous wet surface obtained by scheme 1 has a better fit to the instantaneous incidental wave profile than scheme 2, so the exact instantaneous wetted hull surface can be obtained by scheme 1. Thus, the present method's accuracy is certified.

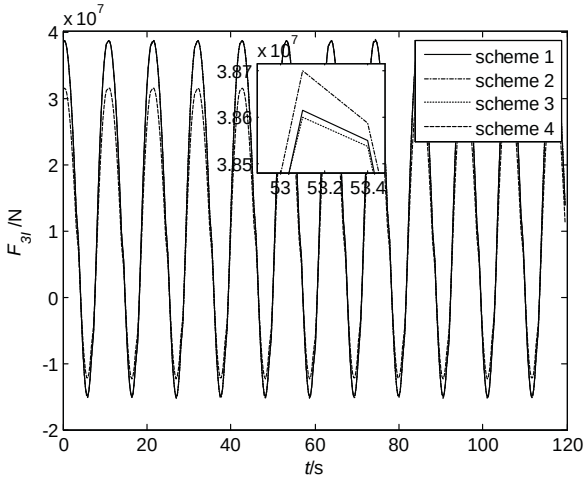

Fig. 12. Time history of heave F-K forces

From Fig. 12, both scheme 1 and scheme 2 show good agreement with scheme 3. But the relative error of the heave F-K force amplitude between scheme 1 and scheme 3 is 0.025%, while the relative error of the heave F-K force amplitude between scheme 2 and scheme 3 is 0.26%. In addition, the relative error of the heave F-K force amplitude between scheme 4 and scheme 3 is -18.47%. Due to the complex curvature of the S175 container ship, the linear method adopted to evaluate F-K forces by scheme 4 leads to larger relative error. Thus, the scheme 1 proposed by the present method is certified.

SHIP MOTIONS RESULTS AND ANALYSIS

The Wigley I hull advances at Froude number Fn=0.2 for λ/L = 1.25 and λ/L = 2.00 in head seas, and the amplitude of the incident wave η_0 is 0.018 m. The non-dimensional heave motion displacement ξ_3' can be defined as $\xi_3' = \xi_3'/\eta_0$, the non-dimensional pitch motion displacement ξ_5' can be defined as $\xi_5' = (\xi_5' L)/(2\pi\eta_0)$, the non-dimensional time t' is defined as t/t_w, and t_w is the wave encounter period. "Linear" denotes the computational results of the linear method, "Present method" denotes the computational results of the proposed method

in this paper, and "RAO" denotes the response amplitude operator.

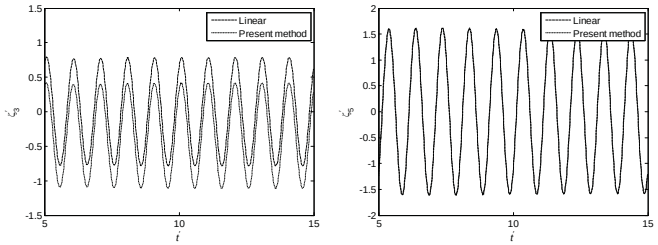

Fig. 13. Time history of non-dimensional heave and pitch motion (λ/L = 1.25)

From Figs. 13~14, the mean position of heave motions using the present method deviates from zero, while the mean position of heave motions by the linear method is also zero. Since the F-K forces and hydrostatic forces are evaluated on the instantaneous wet hull surface, the ship's heave motions are not strictly sinusoidal. The amplitude of pitch motion based on the present method is almost the same as the amplitude of pitch motions based on the linear method for its geometric symmetry around its middle station.

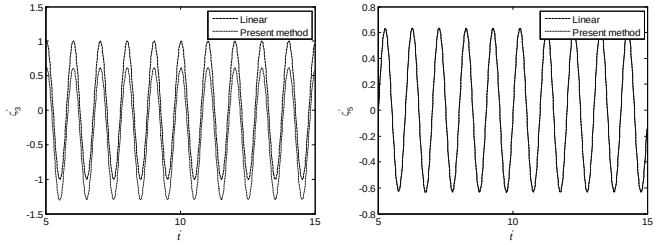

Fig. 14. Time history of non-dimensional heave and pitch motion λ/L = 2.00

In Fig. 15, the "Kim" results are obtained by Kim [8]. The numerical results of heave motion RAO obtained by the present method agree quite well with experimental results for most wavelengths, and the numerical results of pitch motion RAO obtained by the present method are fitted well to the experimental results, except for $\lambda/L = 1.75$. For heave motions, both the present method and the linear method proposed by Kim [8] can obtain better results than the experimental results. For pitch motions, the numerical results by the present method are closer to the experimental results than the linear method. When λ/L approaches 1.75, the numerical results of the pitch response amplitude operator have non-ignorable error compared with the experimental results. When λ/L approaches 1.75, the encounter frequency is nearly equal to the natural frequency of pitch motion, so resonance takes place, and the experimental result is somewhat larger than the numerical result. The present method can incorporate the influences of the curvature of the ship, and the behaviour of the ship in waves could agree well with the experimental results.

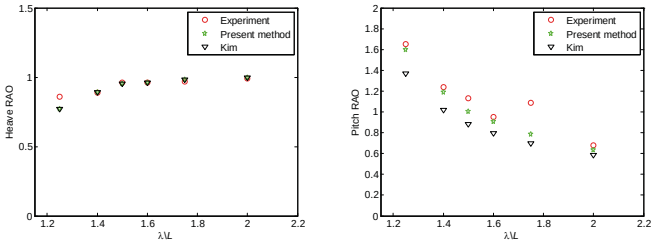

Fig. 15. Heave and pitch motion RAOs

CONCLUSIONS

1) The precise integration method, adopted for the partition computational domain between a small value of time and large value of time, can improve the numerical accuracy substantially. Based on the present method, the TFSGF is applied to solve the radiation problem of a Wigley I hull, and the hydrodynamic coefficients show good agreement with both experimental results and are better than other published results.
2) To evaluate the F-K forces, an adaptive mesh technique based on a quad-tree subdivision is applied to generate the instantaneous wetted hull surface. The panels interacting with the instantaneous wave profile are subdivided by quad-tree subdivision, on which F-K forces are solved by Gauss quadrature, and for panels under the mean free surface, the F-K forces are solved by analytical integration expressions. This process allows for coarser meshes with no loss of accuracy, and the evaluation of the F-K forces could incorporate the influence of the curvature of the hull surface. F-K forces evaluations were carried out with the different methods for an S175 container ship in head waves, and the adaptive mesh technique proposed by this paper obtained better computational results.
3) Comparisons were carried out with both experimental results and a linear method for the ship motions of a Wigley hull in head waves. The numerical results of the present method are in good agreement with the experimental results, especially for the time history of heave motions.

ACKNOWLEDGEMENT

The work is supported by the National Natural Science Foundation of China (Grant No. 51779029); National Social Science Fund (Study on over risk-taking of insurance sector and spillover effect of systemic risks across financial markets: Grant No.17BJY204).

REFERENCES

1. Beck R. F., Liapis S. J. (1983): *Transient motions of floating bodies at zero forward speed.* Journal of Ship Research, 3(31), 164-175.

2. Blandeau F., Francois M., et al. (1999): *Linear and non-linear wave loads on FPSOs.* Proceedings of the ASME

9th International Conference on Offshore Mechanics and Arctic Engineering, France.

3. Clement A. H. (1998): *An ordinary differential equation for the Green function of time-domain free-surface hydrodynamics*. Journal of Engineering Mathematics, 33(2), 201-217.

4. Datta R., Rodrigues J. M., Soares C. G. (2011): *Study of the motions of fishing vessels by a time domain panel method*. Ocean Engineering, 38(5), 782-792.

5. Hess J. L., Smith A. M. O. (1964): *Calculation of non-lifting potential flow about arbitrary three-dimensional bodies*. Journal of Ship Research, 8, 22-44.

6. Huang D. B. (1992): *Approximation of time-domain free surface function and its spatial derivatives*. Journal of Shipbuilding of China, 4, 16-25.

7. Journée J. M. J. (1992): *Experiments and calculations on four Wigley Hull form*. Report 0909, Delft University of Technology.

8. Kim K. H., Kim Y. (2010): *Comparative Study on Ship Hydrodynamics Based on Neumann-Kelvin and Double-Body Linearizations in Time-Domain Analysis*. International Journal of Offshore & Polar Engineering, 10, 265-274.

9. King B. W. (1987): *Time domain analysis of wave exciting forces on ships and bodies*. Report No. 306, University of Michigan.

10. Li Z. F., Ren H. L., Tong X. W., et al. (2015): *A precise computation method of transient free surface Green function*. Ocean Engineering, 105, 318-326.

11. Liu X. M., Zhou G., Zhu S., et al. (2014): *A modified highly precise direct integration method for a class of linear time-varying systems*. China Phys. Mech. Astron., 57, 1382-1389.

12. Magee A. R., Beck R. F. (1988): *Compendium of ship motion calculations using linear time-domain analysis*. Report No. 310, University of Michigan.

13. Rodrigues J. M., Guedes Soares C. (2017): *Froude-Krylov forces from exact pressure integrations on adaptive panel meshes in a time domain partially nonlinear model for ship motions*. Ocean Engineering, 139, 169-183.

14. Sengupta D., Datta R., Sen D. (2016): *A simplified approach for computation of nonlinear ship loads and motions using a 3D time-domain panel method*. Ocean Engineering, 117, 99-113.

15. Shen L., Zhu R. C., Miao G. P., et al. (2007):. *A practical numerical method for deep water time-domain Green function*. Journal of Hydrodynamics, 22(3), 380-386.

16. Singh S. P., Sen D. (2007): *A comparative study on 3D wave load and pressure computations for different level of modelling of nonlinearities*. Marine Structures, 20(1-2), 1-24.

17. Wehausen J. V. (1971): *The motion of floating bodies*. Annual Review of Fluid Mechanics, 3, 237-268.

CONTACT WITH THE AUTHORS

Teng Zhang
e-mail: 1223439945@qq.com
Dalian Maritime University,
1 Linghai Road, 116026 Dalian,
China

Junsheng Ren
e-mail: 1171443834@qq.com
Dalian Maritime University,
1 Linghai Road, 116026 Dalian,
China

Lu Liu
e-mail: j.s.ren@126.com
Dongbei University of Finance and Economics,
217 Jianshan Street, Shahekou District, 116025 Dalian,
China